



PII: S1359-8368(98)00019-5

Analysis and design of sandwich plates with inserts — a high-order sandwich plate theory approach

O.T. Thomsen^a and W. Rits^b

^aInstitute of Mechanical Engineering, Aalborg University, Pontoppidanstraede 101, DK-9220, Aalborg East, Denmark

^bEuropean Space Agency, European Space Research and Technology Centre, Structures and Mechanisms Division, PO Box 299, NL-2200 AG Noordwijk, The Netherlands

(Received 10 November 1997; accepted 10 May 1998)

Sandwich structures are very susceptible to failure due to local stress concentrations induced in areas of load introduction, supports, geometrical and material discontinuities. These local stress concentrations are caused by localised bending effects, where the individual face sheets tend to bend about their own middle surface rather than about the middle surface of the sandwich. This paper deals with such local effects seen around inserts in structural sandwich plates. A high-order theory for bending of sandwich plates, developed and adapted especially for the purpose of studying sandwich plates with inserts and other "hard points", is introduced. The theory, which accounts for the transverse flexibility of the core material, includes separate descriptions of the face sheets and the core materials as well as general specification of loads and boundary conditions. The theory is formulated in terms of first-order partial differential equations, which are solved numerically using the "multi-segment method of integration". Examples involving sandwich plates with "through-the-thickness" inserts subjected to axisymmetric and non-axisymmetric external loading are presented. The paper is concluded by a discussion of design aspects. © 1998 Published by Elsevier Science Ltd. All rights reserved

(Keywords: A. plates; B. buckling)

INTRODUCTION

Structural sandwich elements with metal or FRP face sheets and polymeric foam, Nomex or aluminium honeycomb cores are used extensively for lightweight spacecraft, aircraft and marine structures. The introduction of loads into such structural elements is often accomplished using inserts, which may be of the "through-the-thickness", "fully potted" or "partially potted" types, as illustrated in *Figure 1*.

For all insert types, the ideal load transfer mechanism is disturbed significantly in the regions close to the inserts. In the areas of such disturbances the face sheets will bend locally about their own middle surface rather than about the middle surface of the sandwich panel. This results in severe local stress concentrations in the face sheets, in the core material and in the interfaces between the face sheets and the core. This again might lead to a premature failure, as sandwich panels with transversely flexible cores, such as polymeric foams or honeycombs, are susceptible to failure due to local stress concentrations. Sandwich panels with inserts usually fail owing to delamination, to shear rupture of the core or to direct bending of the face sheets. The local

bending effects causing such structural failures cannot be accounted for using classical "antiplane" sandwich plate theories ("weak core" assumptions), summed up in the monographs by Plantema¹, Allen², Stamm and Witte³ and Zenkert⁴, as such theories do not include the transverse flexibility of the core material. A more advanced transverse bending theory for sandwich plates is presented in the monograph by Librescu⁵, in which sandwich plates with "weak" and "strong" cores are also treated separately. The terms "weak", "antiplane" or "compliant" cores are equivalent concepts and are used to describe an idealised core in which the stretching and shearing stiffnesses in planes parallel with the face sheets are zero but the shear modulus perpendicular to the face sheets is finite^{2,4,5}. This is in contrast to a sandwich panel with a strong core (or rigid core) which is characterized by the fact that the core inplane stretching and shearing stiffnesses are taken into account ⁵. For most structural sandwich panel applications the weak core assumptions can be adopted, since very lightweight core materials such as polymeric foams and honeycombs are usually used.

In the theory developed by Librescu⁵ the sandwich panels treated are assumed to be symmetric and the core material is

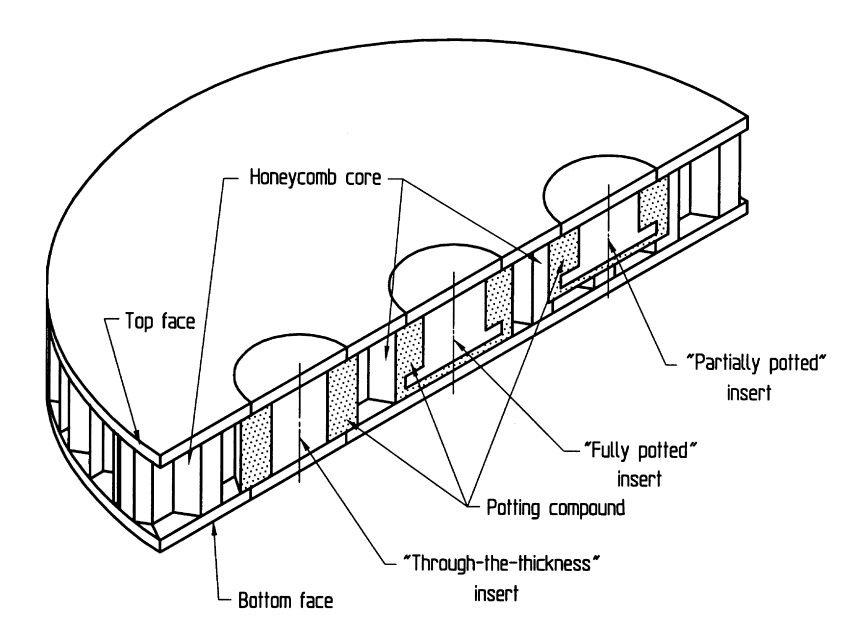


Figure 1 Insert types typically used for structural sandwich panels

modelled as a moderately thick plate, where the presence of core transverse normal stresses is included in the modelling. The sandwich plate model presented in Ref. 5 does not, however, include the transverse flexibility of the core material, since it is assumed *a priori* that the transverse deflection of the core is uniform through the core thickness (i.e. the core transverse normal strain $\varepsilon_z = 0$).

The importance of including the transverse flexibility of the core (i.e. allowing the core thickness to change during deformation of the sandwich panel) when addressing load introduction problems, support problems, and problems involving material and geometric discontinuities in sandwich beams was pointed out by Frostig and coworkers^{6–8}. This was done by formulating a "high-order" sandwich beam theory, which includes a separate description of each face sheet and a separate description of the core material. The core material is modelled as a special type of transversely isotropic solid where only the out-of-plane stiffness is accounted for. In other words, the core type considered in Refs. 6–8 is a transversely isotropic weak core where the plane of isotropy is parallel to the core middle plane.

This paper addresses the problem of analysis of sandwich plates with inserts of the through-the-thickness type (see *Figure 1*). The problem is formulated by adapting and extending the principles behind the sandwich theory developed for sandwich beams in Refs. 6–8 to sandwich plates. Full details about the mathematical formulation can be found in Refs. ^{9,10} for sandwich plates with through-the-thickness and fully potted inserts.

MATHEMATICAL FORMULATION

Model definition

In the modelling of the insert-sandwich plate system it is assumed that the interaction between adjacent inserts, as

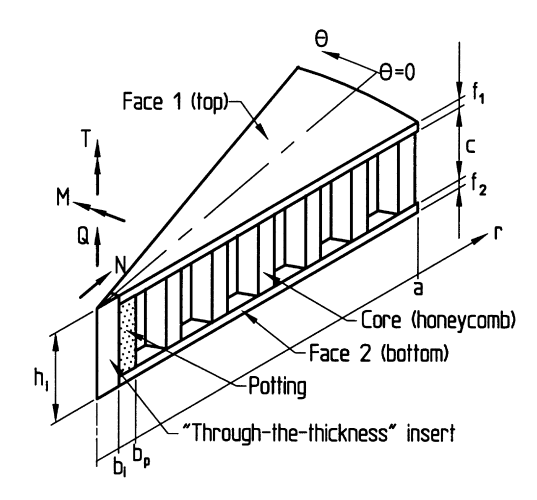


Figure 2 Definition of circular sandwich plate with "through-the-thickness" insert

well as the interaction between an insert and the plate boundaries or other sources of local disturbances, can be ignored. *Figures 2* and *3* define the constituent parts, the geometry and the possible external load cases. The sharp interface between the potting and the honeycomb indicated in *Figure 2* represents a strong idealisation, as the "real" potting—honeycomb intersection is not defined precisely in a geometrical sense.

The following restrictive assumptions are adopted in the formulation:

- the face sheets are modelled as elastic plates including, and the effects of transverse shearing deformations may be accounted for. Furthermore, the face sheets are treated as homogeneous, isotropic and linear elastic;
- the sandwich plate can be asymmetric, i.e. the face sheets may have unequal thicknesses (see *Figure 3*) and unequal elastic properties;
- the core material in both the potting and honeycomb regions is assumed to behave as a special type of

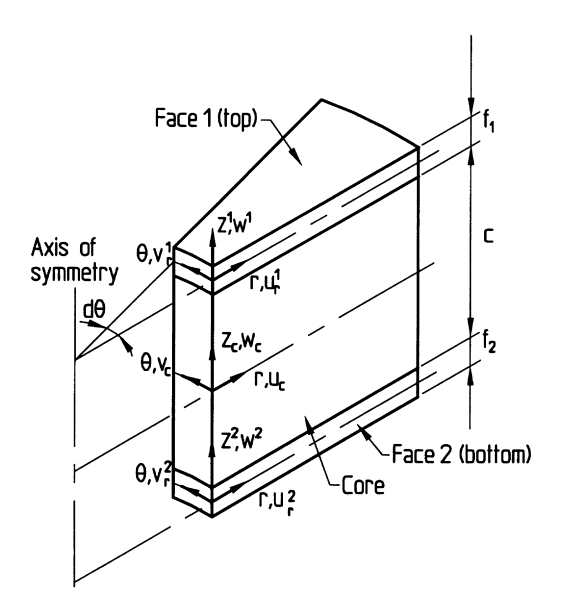


Figure 3 Geometrical definition of sandwich plate element consisting of top face sheet (face 1), core material (potting and honeycomb materials) and bottom face sheet (face 2)

transversely isotropic material only possessing stiffness in the through-the-thickness direction (z_c -direction, see *Figure 3*), where the plane of isotropy is parallel to the middle plane of the core;

Considering the conditions for equilibrium in the core material, the following relations can be established:

$$\tau_{rz,z} = 0
\tau_{\theta z,z} = 0
\sigma_{c,z} + \tau_{rz,r} + \frac{1}{r} \tau_{rz} + \frac{1}{r} \tau_{\theta z,\theta} = 0$$
(2)

where differentiation with respect to the spatial coordinates is denoted by a subscript comma. This convention is adopted throughout the paper. In eqn (2) σ_c is the core transverse normal stress, and τ_{rz} and $\tau_{\theta z}$ are the core shear stress components. From the first two equations in eqn (2), it follows directly that the core shear stress components are independent of the z_c -coordinate. The equations in eqn (2) are identical with the core equilibrium equations obtained by Librescu⁵, because the same weak core assumptions have been adopted *a priori*.

Combination of the core equilibrium equations, eqn (2), with the core kinematic and constitutive relations yields a set of equations describing the complete core stress and displacement fields in terms of the transverse core coordinate $z_{\rm c}$ (measured from the core middle plane) and in terms of the face sheet displacement components. The complete derivations are presented in Appendix A, and the resulting core equations read:

$$\tau_{rz}(r, \theta, z_{c}) = \tau_{rz}(r, \theta)
\tau_{\theta z}(r, \theta, z_{c}) = \tau_{\theta z}(r, \theta)
\sigma_{c}(r, \theta, z_{c}) = \frac{E_{c}}{c} \left\{ w^{1} - w^{2} \right\} - \left\{ \tau_{rz, r} + \frac{1}{r} \tau_{rz} + \frac{1}{r} \tau_{\theta z, \theta} \right\} z_{c}
w_{c}(r, \theta, z_{c}) = w^{1} + \frac{\left\{ w^{1} - w^{2} \right\}}{c} \left\{ z_{c} - \frac{c}{2} \right\} - \frac{1}{2E_{c}} \left\{ \tau_{rz, r} + \frac{1}{r} \tau_{rz} + \frac{1}{r} \tau_{\theta z, \theta} \right\} \left\{ z_{c}^{2} - \frac{c^{2}}{4} \right\}
u_{c}(r, \theta, z_{c}) = u_{0r}^{1} + \frac{w_{, r}^{1}}{2} \left\{ f_{1} - \frac{z_{c}^{2}}{c} - z_{c} + \frac{3c}{4} \right\} + \frac{w_{, r}^{2}}{2} \left\{ \frac{z_{c}^{2}}{c} - z_{c} + \frac{c}{4} \right\} + \frac{\tau_{rz}}{G_{c}} \left\{ z_{c} - \frac{c}{2} \right\}
+ \frac{1}{2E_{c}} \left\{ \tau_{rz, rr} + \frac{1}{r} \tau_{rz, r} - \frac{1}{r^{2}} \tau_{rz} + \frac{1}{r} \tau_{\theta z, \theta r} - \frac{1}{r^{2}} \tau_{\theta z, \theta} \right\} \left\{ \frac{z_{c}^{3}}{c} - \frac{c^{2} z_{c}}{4} + \frac{c^{3}}{12} \right\}
v_{c}(r, \theta, z_{c}) = u_{0\theta}^{1} + \frac{w_{, \theta}^{1}}{2r} \left\{ f_{1} - \frac{z_{c}^{2}}{c} - z_{c} + \frac{3c}{4} \right\} + \frac{w_{, \theta}^{2}}{2r} \left\{ \frac{z_{c}^{2}}{c} - z_{c} + \frac{c}{4} \right\} + \frac{\tau_{\theta z}}{G_{c}} \left\{ z_{c} - \frac{c}{2} \right\}
+ \frac{1}{2rE_{c}} \left\{ \tau_{rz, r\theta} + \frac{1}{r} \tau_{rz, \theta} + \frac{1}{r} \tau_{\theta z, \theta \theta} \right\} \left\{ \frac{z_{c}^{3}}{c} - \frac{c^{2} z_{c}}{4} + \frac{c^{3}}{12} \right\}$$
(3)

 the top and bottom face sheets may deflect differently, i.e. no assumptions about the sandwich plate displacement field are adopted a priori.

Derivation of core equations

As a direct consequence of the weak core assumptions adopted, there can be no transfer of in-plane stresses in the core material, i.e.

$$\sigma_r = \sigma_\theta = \tau_{r\theta} \equiv 0 \tag{1}$$

In eqn (3) $E_{\rm c}$ and $G_{\rm c}$ are the core elastic constants, $u_{\rm c}$, $v_{\rm c}$ and $w_{\rm c}$ are the radial, circumferential and transverse displacement components of the core material; u^i_{0r} , $u^i_{0\theta}$ and w^i (i=1,2) are the radial, circumferential and transverse displacement components of the top and bottom faces; r and θ are the radial and circumferential coordinates.

From eqn (3) it is noticed that τ_{rz} and $\tau_{\theta z}$ do not vary across the core thickness. It is further seen that σ_z varies linearly, that w_c varies quadratically, and finally that u_c and v_c vary cubically over the thickness of the core.

The core material response is coupled with the face sheet

responses by requiring continuity of the displacement field across the core—face sheet interfaces. This implies that the following surface tractions and shear stresses are transferred between the core and the face sheets:

top face-core interface:

$$\sigma_{\rm c}^{\rm top} = \sigma_{\rm c}(r, \, \theta, \, c/2)$$
 (4a)

$$\tau_{rz} = \tau_{rz}(r, \ \theta) \tag{4b}$$

$$\tau_{\theta z} = \tau_{\theta z}(r, \ \theta) \tag{4c}$$

bottom face-core interface:

$$\sigma_{\rm c}^{\rm bottom} = \sigma_{\rm c}(r, \, \theta, \, -c/2)$$
 (4d)

$$\tau_{rz} = \tau_{rz}(r, \ \theta) \tag{4e}$$

$$\tau_{\theta_{\bar{z}}} = \tau_{\theta_{\bar{z}}}(r, \ \theta) \tag{4f}$$

Derivation of the complete set of governing equations

The face sheets are modelled as elastic plates, with the possibility of including transverse shearing effects in the modelling. Thus, the plate model adopted corresponds to a Mindlin–Reissner type of plate theory. In cases where the face sheets are thin, the transverse shearing effects in the face sheets themselves can be ignored compared with the transverse shearing of the core material. In the actual case, the degrees of freedom corresponding to the rotation of the normals to the face sheet middle surfaces were locked, and consequently the modelling of the face sheets was achieved using a Love–Kirchhoff type of plate theory.

Formulation of the equilibrium, kinematic and constitutive equations for the top and bottom face sheets, and combination of those with the core equations (eqn (3)) and continuity requirements (eqns (4)), yields the governing set of differential equations. It turns out that in this formulation the order of the set of governing equations is 24, since the necessary number of boundary conditions to be specified along an edge is 12. Consequently, the governing equations can be reduced to 24 first-order partial differential equations with 24 unknowns. If the 24 unknowns, henceforth called the fundamental variables, are those quantities that appear in the natural boundary conditions at an edge r = constant, then the boundary value problem can be stated completely in terms of these variables. In the present case, the 24×1 matrix of fundamental variables can be written as

$$\{y(r, \theta)\} = \{u_{0r}^{1}, u_{0\theta}^{1}, w^{1}, \beta_{r}^{1}, \beta_{\theta}^{1}, N_{r}^{1}, N_{r\theta}^{1}, M_{r}^{1}, M_{r\theta}^{1}, M_{r\theta}^{2}, M_{r\theta}^{2},$$

where β_r^i and β_θ^i are the rotations of the normals to face sheet midsurfaces, N_r^i and $N_{r\theta}^i$ are the face sheet in-plane stress resultants, M_r^i and $M_{r\theta}^i$ are the face sheet moment resultants,

and Q_r^i are the face sheet radial transverse shear stress resultants (i=1,2). In eqn (5) two new "core variables" q_r and q_θ have been introduced:

$$q_r(r, \theta) = \tau_{rz,r}, \quad q_{\theta}(r, \theta) = \tau_{r\theta,r}$$
 (6)

Adopting the matrix of fundamental variables $\{y(r, \theta)\}$, the governing equations can be reduced to the form

$$\{y(r, \theta)\}_{r} = \Psi(r, \theta, \{y\}, \{y\}_{\theta}, \{y\}_{\theta\theta}, ...)$$
 (7)

where Ψ denotes 24 linear functions in $\{y(r,\theta)\}$ and its derivatives with respect to θ . The complete set of governing equations (including the equations for the top face sheet, the core and the bottom face sheet) is given in Appendix B. As is seen from the complete set of governing equations given in Appendix B, transverse bending and in-plane stretching effects are coupled in the derived high-order sandwich plate theory. This is a consequence of the interaction between the two face sheets through the core material, through which shearing and transverse normal stresses are transferred.

The dependency of the θ -coordinate is eliminated by Fourier series expansion of the fundamental variables, thus reducing the problem to two sets of 24 first-order ordinary differential equations. In abbreviated form the complete set of Fourier series expanded set of governing equations can be specified in the form:

symmetric about $\theta = 0$:

$$\{y_n(r)\}_{,r} = [A_n(r)]\{y_n(r)\} + \{B_n(r)\}, \qquad n = 1 \to \infty$$
 (8a)

skew-symmetric about $\theta = 0$:

$$\{\tilde{y}_n(r)\}_{,r} = [\tilde{A}_n(r)]\{\tilde{y}_n(r)\} + \{\tilde{B}_n(r)\}, \qquad n = 1 \to \infty$$
 (8b)

where $\{y_n(r)\}$, $\{\tilde{y}_n(r)\}$ are 24×1 matrices of r-dependent coefficient functions of the Fourier series expanded vector of fundamental variables; $[A_n(r)]$ and $[\tilde{A}_n(r)]$ are 24×24 coefficient matrices; $\{B_n(r)\}$, $\{\tilde{B}_n(r)\}$ are 24×1 matrices of nonhomogeneous load terms.

Specification of boundary conditions

The actual statement of the boundary conditions varies somewhat from load case to load case (Q, T, M or N), see $Figure\ 2$, but with reference to $Figure\ 2$ the imposed boundary conditions are generally derived from the following assumptions:

- r = b_i: the through-the-thickness insert is considered as an infinitely rigid body to which the face sheets and the potting material are rigidly connected;
- r = b_p: continuity of the fundamental variables across the potting-honeycomb interface;
- r = a: it is assumed that the face sheet and honeycomb core midsurfaces are simply supported.

Generally, the boundary conditions at $r = b_i$ and r = a are stated by specifying linear combinations of the fundamental variables, i.e.

symmetric about $\theta = 0$:

$$[T_n^{b_i}]\{y_n(r=b_i)\} = \{Y_n^{b_i}\}$$
 (9a)

$$[T_n^a]{y_n(r=a)} = {Y_n^a}$$
 (9b)

skew-symmetric about $\theta = 0$:

$$[\tilde{T}_{n}^{b_{i}}]\{\tilde{y}_{n}(r=b_{i})\} = \{\tilde{Y}_{n}^{b_{i}}\}$$
 (9c)

$$[\tilde{\boldsymbol{T}}_{n}^{a}]\{\tilde{\boldsymbol{y}}_{n}(r=a)\} = \{\tilde{\boldsymbol{Y}}_{n}^{a}\} \tag{9d}$$

where $[\boldsymbol{T}_n^i]$, $[\tilde{\boldsymbol{T}}_n^i]$ $(i=b_i,a)$ are 24×24 non-singular transformation matrices, and $\{Y_n^i\}$, $\{\tilde{Y}_n^i\}$ $(i=b_i,a)$ are 24×1 matrices containing the fundamental variables at $r=b_i$ and r=a (and thereby also the 12 prescribed boundary conditions at each location). It should be emphasized that the form of eqns (9) does not involve any restrictions on the boundary conditions, and that any geometric or natural boundary conditions can be stated in this form.

Numerical solution: multi-segment method of integration

The sets of governing equations (eqns (8)) together with the statement of the boundary conditions (eqns (9)) constitutes a boundary value problem. No general closed form solution for this problem is available, and a numerical solution scheme was therefore developed.

In the present case the boundary value problem was solved numerically using the "multi-segment method of integration". This method offers the following features:

- it is easy to implement;
- it can be applied conveniently to systems of first-order ordinary differential equations;
- it permits arbitrary radial variations, including discontinuities, of all the dependent variables of the problem.

Without giving the details, the method is based on a transformation of the boundary value problem into a series of interconnected initial value problems. The insertsandwich plate configuration is divided into a finite number of segments, and the solution within each segment is derived by direct integration (simultaneous integration of $24 \times 24 = 576$ first-order differential equations). Continuity of the solution vectors $(\{y_n(r)\}, \{\tilde{y}_n(r)\})$ across the separation points between the segments, as well as fulfilment of the boundary conditions at $r = b_i$ and r = a, is ensured by formulating and solving a set of linear algebraic equations. Further details about the multi-segment method of integration can be found in Ref. 11. The implementation of the numerical solution scheme was accomplished using a UNIX-version of MATLAB $^{\circ}$, version 4.1, installed on an HP9000/700 work station. The direct integration was carried out using an adaptive step-size fourth- and fifthorder Runge-Kutta-Fehlberg method. Detailed information about the applied numerical solution scheme can be found in Ref. 9.

IMPLICATIONS AND LIMITATIONS OF THE DEVELOPED THEORY

The face sheets are treated as homogeneous, isotropic and linear elastic. Obviously, this is a simplifying assumption as the face sheets are often made as FRP-laminates. However, the adopted approximation is quite reasonable in reality, since strongly orthotropic face-laminates are hardly ever used around inserts or other areas of load introduction. Instead, if the surrounding sandwich structure is made with strongly orthotropic face-laminates, the zones around the inserts will be reinforced locally such that the resulting laminates appear as nearly quasi-isotropic with respect to the in-plane properties. For the cases where slightly orthotropic face sheets are used, the present formulation will provide sufficiently accurate results if the engineering constants E_i and ν_i^2 of the face sheets are replaced by effective quantities defined by 12 :

$$(E_{i})_{\text{eff}} = \sqrt{E_{xi}E_{yi}}$$

$$(\nu_{i}^{2}) = \nu_{xi}\nu_{yi}$$

$$(i = 1, 2)$$
(10)

where subscripts x and y denote principal material directions. For the rare cases where strongly orthotropic face-laminates are used, the model in its present form is not applicable. However, it is possible to include orthotropic face sheet properties in the formulation.

The honeycomb core material is modelled as being a homogeneous, isotropic and linear elastic material which supplies a continuous support for the face sheets. This is in conflict with the physical problem on two points. Firstly, the hexagonal cell structure of honeycombs results in orthotropic in-plane properties. However, orthotropic core properties can be included in the formulation. Secondly, the discrete cellular nature of honeycomb materials has been excluded from the analysis, as the honeycomb properties are effectively "smeared out" over the honeycomb cell areas. Thus, the stresses obtained for the honeycomb material should be considered as "averaged" over the honeycomb cell areas. Consequently, the actual load transfer mechanisms in the cell walls of the honeycomb core are not reflected by the "average" core stresses obtained. The core stresses obtained, however, comply well with the "smeared" or overall stiffness and strength properties supplied by the manufacturers of honeycombs.

Finally, it should be noted that the sharp separation between potting and honeycomb assumed in the modelling represents on idealisation. In reality the potting—honeycomb intersection is highly irregular, as it is created when the potting compound flows into those honeycomb cells which have been left open during machining in preparation of the insert hole. This problem can only be surmounted by adopting a model which accounts for the discrete nature of the cellular honeycomb materials.

Pertaining to a comparison between the suggested highorder sandwich plate theory relative to classical antiplane sandwich theories^{1–4}, the following comparative features should be highlighted:

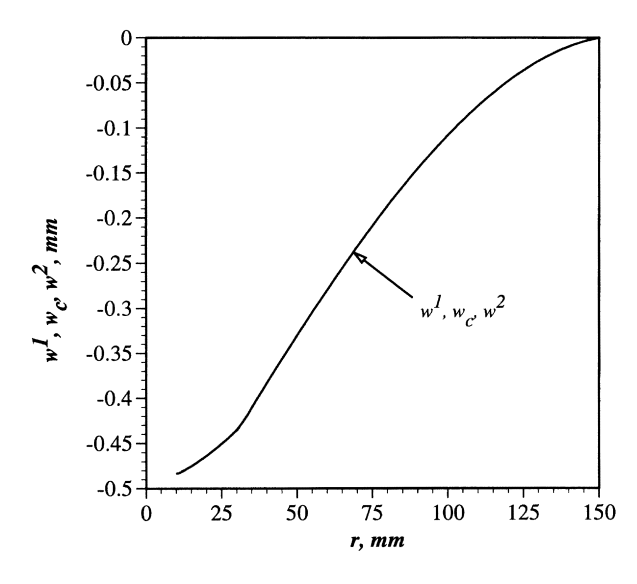


Figure 4 Lateral displacements w^1 , w^2 , $w_c(z_c = 0)$. Q = -1.0 kN

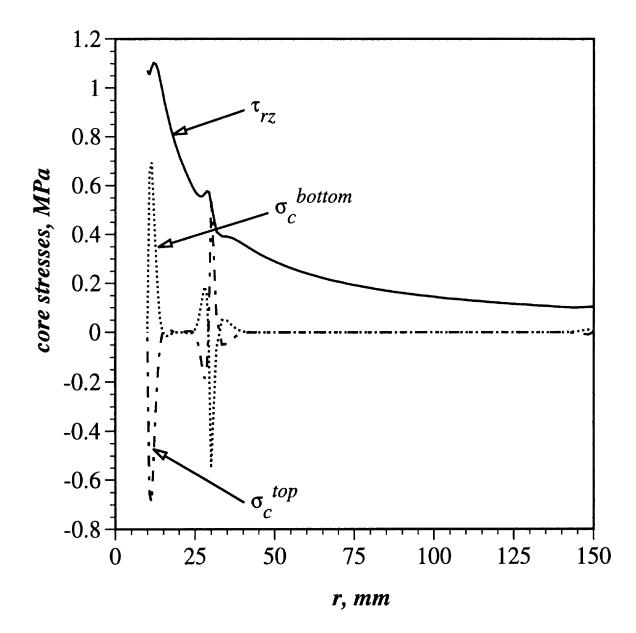


Figure 5 Core stress components τ_{rz} , σ_{c}^{top} , σ_{c}^{bottom} . Q = 1.0 kN

- The suggested high-order theory supplies information about the displacement fields of each face sheet, as well as of each point in the core material. The core displacements are predicted to vary non-linearly through core thickness.
- As opposed to this, classical antiplane theories assume the core thickness to be constant. Consequently, the in-plane core displacements are predicted to vary linearly over the core thickness.
- Both types of theory assume that the core shear stresses are constant through the core thickness (consequences of neglecting the in-plane stretching and shearing core stiffnesses), and there is very little difference between the predicted values. However, the high-order sandwich plate theory accounts for the existence of transverse normal stresses in the core material. The transverse normal core stresses will in many cases play an important role in the onset and development of failure.

EXAMPLES

In the following some numerical results for the case of sandwich plates with through-the-thickness inserts are presented. Two important load cases are discussed:

- (1) out-of-plane load Q (axisymmetric), see Figure 2;
- (2) bending moment loading M (non-axisymmetric), see Figure 2. The discussion of the two load cases will be based on the same geometry and material data:

Geometry: $b_i = 10 \text{ mm}, b_p = 30 \text{ mm}, a = 150 \text{ mm}, c =$

10 mm, $f_1 = f_2 = 1$ mm.

quasi-isotropic FRP-laminate with properties Top face:

 $E_{\rm fl} = 40$ GPa, $\nu_{\rm fl} = 0.3$.

Bottom face: as top face, i.e. $E_{\rm f2}=E_{\rm f1}$, $\nu_{\rm f2}=\nu_{\rm f1}$.

bulk epoxy, $E_p = 2.5$ GPa, $G_p = 0.93$ GPa. Potting compound:

Hexcel honeycomb 3/16''-5056-0.0007'', $E_h =$ Honeycomb core:

310 MPa, $G_h \approx (G_W + G_L)/2 = 138$ MPa.

Out-of-plane loading (Q load case)

The case of external out-of-plane loading Q is probably the most important of all the load cases, and design guidelines for this load case can be found in Ref. 12 for instance. However, no elaborate description of the deformation patterns and stress distributions are given in Ref. 12, and the guidelines specified do not supply detailed insight into the mechanics of the sandwich plate-insert problem.

In the example presented it is assumed that Q = -1.0 kN(i.e. "comprehensive" out-of-plane loading).

Figure 4 shows, the lateral deflections of the face sheets (w^1, w^2) , and the core midsurface $(w_c(z_c = 0))$.

In Figure 4 (and the figures to come) it is noticed that $r \le$ $b_p = 30$ mm corresponds to the potting region, whereas r >30 mm corresponds to the honeycomb region. From the results displayed, it is seen that the lateral deflections of the two face sheets and the core material midsurface are almost identical. As expected, owing to the symmetry of the sandwich plate considered, the lateral displacements of the two face sheets w^1 and w^2 are identical. The midsurface lateral displacement of the core material w_c (potting and honeycomb), however, is slightly different from w^1 and w^2 close to the insert-potting and potting/honeycomb interfaces (difficult to see from the figure) where the core properties change abruptly. The differences between the lateral face sheet displacements and core displacements, encountered at these locations, causes the inducement of transverse normal stresses (σ_c) in the potting and the honeycomb core.

Figure 5 shows the stress distribution in the core material. The values of the transverse normal stress σ_c are given at the interface between the top face sheet and the core (σ_c^{top}) , as well as at the interface between the bottom face sheet and the core $(\sigma_c^{\text{bottom}})$. According to the high-order sandwich plate theory σ_c varies linearly over the core thickness, see eqn (3). Figure 5 also shows the distribution of the

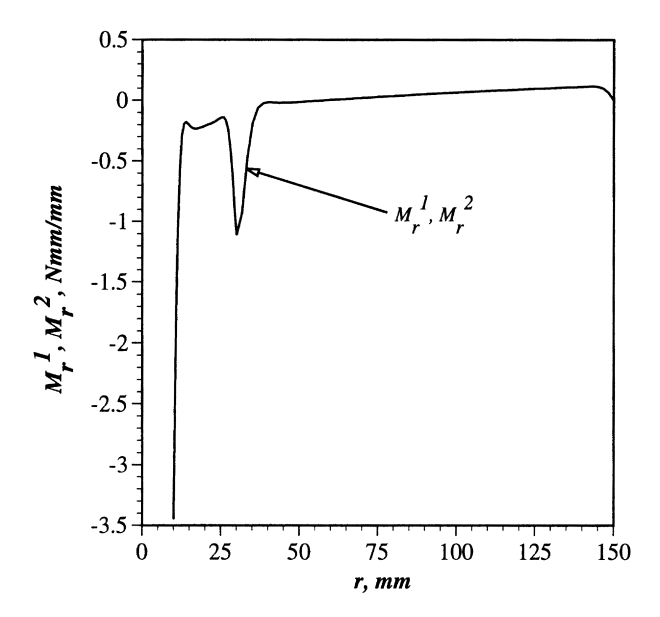


Figure 6 Radial bending moment resultants M_r^1 , M_r^2 . Q = 1.0 kN

transverse core shear stress component τ_{rz} , which is assumed to be constant over the height of the core material, see eqn (3).

Considering the σ_c -distribution, it is observed that the presence of transverse normal stresses is a very local phenomenon, as significant σ_c -contributions are only present close to $r=b_i=10$ mm (i.e. close to the insert) and close to $r=b_p=30$ mm (i.e. close to the potting-honeycomb intersection). It is seen that σ_c^{top} and σ_c^{bottom} are of opposite signs, i.e. when one is compressive the other is tensile and vice versa.

Considering the shear stress distribution in the core material, the overall tendency is that τ_{rz} decreases with increasing r-values. The overall tendency of decreasing τ_{rz} -values with increasing r is a consequence of the fact that the total transverse shear stress resultant $Q_r^{\rm total} = Q_r^1 + Q_r^2 + c\tau_{rz}$ is inversely proportional to r (vertical equilibrium requires $Q = 2\pi r Q_r^{\rm total}$), and that the main part of Q is carried by the core material (i.e. by τ_{rz}). It is further seen from Figure~5 that the abrupt change of core stiffness at the potting–honeycomb intersection only causes minor fluctuations of the τ_{rz} -distribution.

Considering the combined influence of the transverse normal and the shear stress components on the potting and honeycomb materials, it should be noticed that the mechanical properties of the two materials are very different¹². Thus, the stiffness and strength properties of the honeycomb material are usually an order of magnitude lower than those of the potting.

Recalling from *Figure 5*, that the magnitudes of the peak stresses in the potting and honeycomb regions are about the same, it is then seen that a "weak spot" is located at the position of the potting–honeycomb intersection (at $r = b_p$) as well as a short distance into the honeycomb material.

From this, it is concluded that the stress concentrations in the potting region (closest to the insert) are not likely to cause a failure, except for the possibility of failure due to weak bonds between the insert and the potting as well as between the face sheets and the potting.

However, the stress concentrations encountered at the potting honeycomb intersection, and immediately after that, might cause a premature failure. The active failure mechanisms could be one of three.

Top-surface of honeycomb:

the tensile σ_c^{top} stresses might cause a failure in the (weak) bond between the top face sheet and the honeycomb.

Potting-honeycomb intersection:

the τ_{rz} stresses might cause a shear rupture of the core surrounding the potting material.

Bottom-surface of honeycomb:

the compressive σ_c^{bottom} stresses might cause a compression failure (buckling) of the honeycomb cells.

In practice, core shear rupture of the undoubled core foils is the cause of structural failure in most cases, i.e. shear failure occurs at the potting-honeycomb intersection ¹².

Figure 6 shows the distribution of the radial bending moment resultants M_r^1 and M_r^2 . It is observed that M_r^1 and M_r^2 are identical (owing to the symmetry of the sandwich plate considered) and that they attain their peak values at the insert–potting intersection ($r = b_i = 10$ mm). The location of the peak bending moment resultants at this location is due to the restrictive boundary conditions imposed by the insert.

Another local peak is seen around the potting-honey-comb intersection at $r = b_p$ but the decay of M_r^1 and M_r^2 is seen to be complete a short distance away from $r = b_p$.

The results presented demonstrate that complicated load transfer mechanisms are active in sandwich plates with inserts. This is especially pronounced in the regions close to the insert, and close to the potting-honeycomb interface, i.e. in regions where significant changes of geometry and stiffness properties take place. Away from the locations of discontinuous change of geometry or material properties, the core material carries the load in pure shear and no local stress concentrations are present. In these regions, classical antiplane sandwich plate theory¹⁻⁴ is capable of describing the stress state accurately.

Bending moment loading (M load case)

To further demonstrate the capabilities of the developed high-order sandwich plate theory, an example of a circular sandwich plate with a through-the-thickness insert subjected to an external bending moment M (non-axisymmetric load case; see $Figure\ 2$) is presented. The bending moment load case is highly realistic, even though it is generally recommended to avoid this load type through proper design (using groups of inserts instead of just one insert). The geometry and material data are assumed to be the same as for the Q load case. The external bending moment is assumed to be $M=25\ N$ m, and is imposed by rotating the though-the-thickness insert as a rigid body about the core midsurface.

Figure 7 shows w^1 , w^2 and w_c (midsurface) = $w_c(z_c = 0)$ along $\theta = 0$ (varies as $\cos(\theta)$, see Figure 2). The lateral deflections w^1 and w^2 of the two face sheets, as well as the lateral deflection of the core midsurface $w_c(z_c = 0)$, are slightly different from each other except at $r = b_i = 10$ mm and r = a = 150 mm owing to the imposed boundary conditions.

A characteristic feature of the results shown in *Figure 7* is the abrupt change of sign of the deflection "slope", which is seen around $r=b_{\rm p}=30$ mm, i.e. at the potting-honeycomb intersection.

Figure 8 shows a surface plot of the deflectional response of the top face sheet of the insert–sandwich plate system. The deformed face sheet is symmetric about $\theta = 0$ ($\theta = 0$ is coincident with the x-axis in Figure 8) and, therefore, only one half of the deformed face sheet is shown. The central

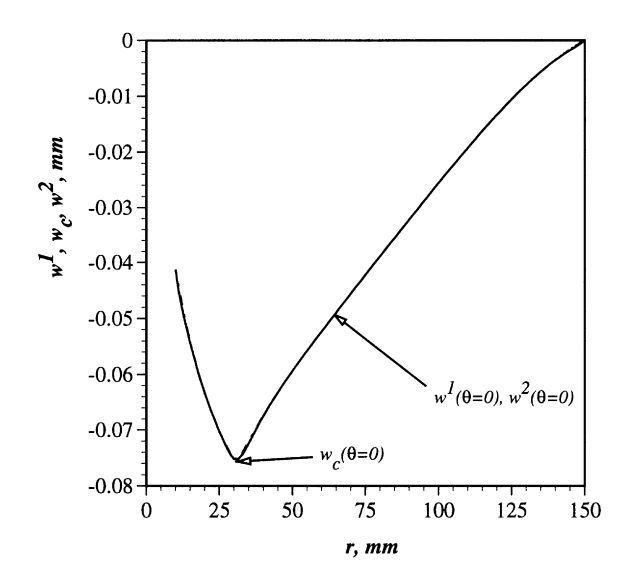


Figure 7 Lateral displacements $w^1(\theta = 0)$, $w^2(\theta = 0)$, $w_c(z_c = 0, \theta = 0)$. M = 25 N m

part of the deformed top face sheet, extending from (x, y) = (0, 0) to $r = (x^2 + y^2) = b_i = 10$ mm in all directions corresponds to the rigid through-the-thickness insert.

Figure 9 shows the distribution of stresses in the core material (potting and honeycomb), and the close resemblance with the core stress distribution for the Q load case (displayed in Figure 5) should be noted. Four stress components are shown; $\sigma_{\rm c}^{\rm top}$, $\sigma_{\rm c}^{\rm bottom}$ and $\tau_{\rm rz}$, which are given along $\theta=0$ (they vary as $\cos(\theta)$), and $\tau_{\theta z}$, which is given along $\theta=\pi/2$ (varies as $\sin(\theta)$). It is seen that significant peaks of the transverse normal stresses $\sigma_{\rm c}^{\rm top}$ and $\sigma_{\rm c}^{\rm bottom}$ are present close to the insert $(r=b_{\rm i})$ and around the potting-honeycomb intersection $(r=b_{\rm p})$.

It should be noted that the absolute values of σ_c^{top} and σ_c^{bottom} are not the same. The reason for this "asymmetric" behaviour (not even "skew symmetric" about the core midsurface) is that the stress states in the two face sheets are not identical, thus causing an asymmetric core stress distribution to appear.

The presence of $\tau_{\theta z}$ is a consequence of the non-axisymmetric nature of the M load case. It is observed that $\tau_{\theta z}$ builds up and attains its peak value approximately in the middle of the potting (at $r \approx 20$ mm). It should be noted that σ_c^{top} , σ_c^{bottom} and τ_{rz} attain their peaks along $\theta = 0$ and $\theta = \pi$, whereas $\tau_{\theta z}$ attains its peak values for $\theta = \pi/2$ and $\theta = 3\pi/2$. It is therefore concluded that the peaks of σ_c^{top} , σ_c^{bottom} and τ_{rz} never occur at the same locations as the peaks of $\tau_{\theta z}$. Pertaining to the combined influence of the transverse normal and shear stress components on the potting and honeycomb materials, reference is made to the comments given for the Q load case.

Figure 10 shows the radial bending moment resultants M_r^1 and M_r^2 along $\theta=0$ (M_r^1 and M_r^2 vary as $\cos(\theta)$). It is seen that the magnitudes of the bending moment resultants in the two face sheets are dissimilar. Around the potting-honeycomb intersection at $r=b_p=30$ mm a characteristic "disturbance" of the M_r^i distributions is seen.

For examples involving sandwich plates with throughthe-thickness inserts subjected to other types of external

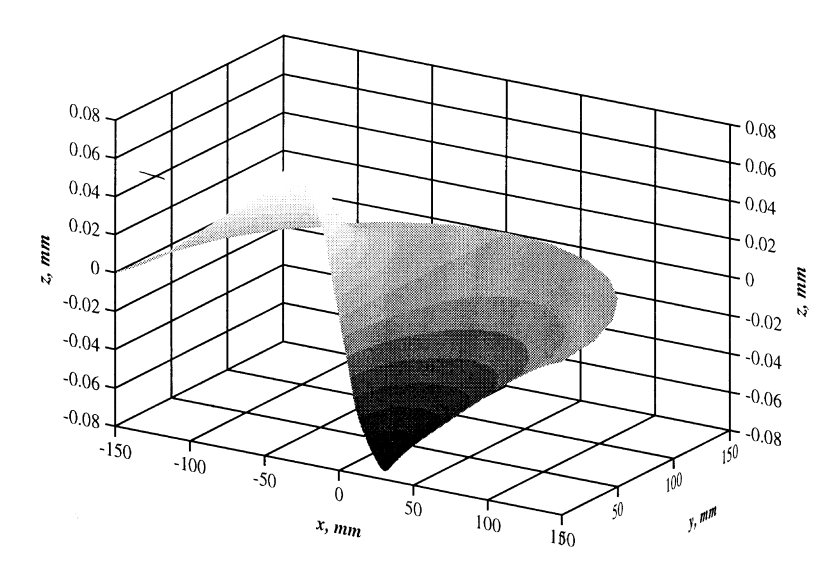


Figure 8 Surface plot of the deformed top face sheet (one half shown). M = 25 N m

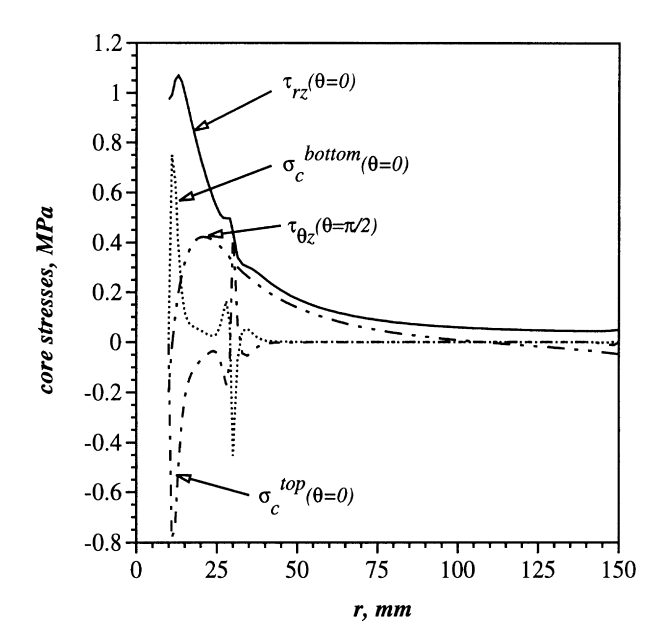


Figure 9 Core stress components $\sigma_c^{\text{top}}(\theta=0)$, $\sigma_c^{\text{bottom}}(\theta=0)$, $\tau_{rz}(\theta=0)$, $\tau_{\theta z}(\theta=\pi/2)$. M=25 N m

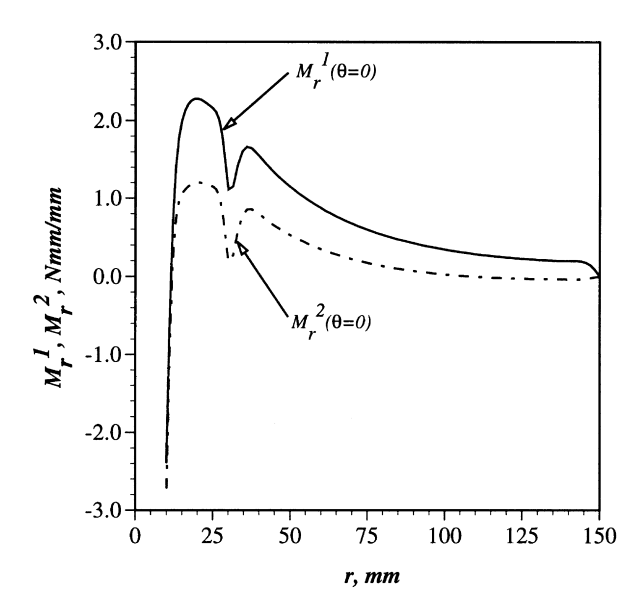


Figure 10 Radial bending moment resultants $M_r^1(\theta=0)$, $M_r^2(\theta=0)$. M = 25 N m

loading (see *Figure 2*) and sandwich plates with fully potted inserts (see *Figure 1*) see Refs. 9,10.

DISCUSSION OF DESIGN ASPECTS

Comparing *Figures 5* and *6* for the out-of-plane load case, and *Figures 9* and *10* for the bending moment load case, it should be recognised that the potting compound plays an important structural role in the overall load transfer around the insert.

Obviously, the "primary" function of the potting material is to provide the connection between the insert and the

honeycomb material, or, in other words, to ensure that a proper shear load transfer can be accomplished between the insert and the honeycomb material. This connecting function is obtained when the potting compound is injected and flows into those honeycomb cells that have been left open during machining (in preparation of the hole for the insert).

The other, or "secondary", function of the potting material is associated with its participation in the overall load transfer, and is less obviously recognised than the simple connecting function mentioned above. Thus, the potting compound plays a significant role in the load transfer in insert–sandwich plate systems, especially those subjected to "transverse" load types (i.e. Q and M load cases, see Figure 2). The presence of a potting compound, which is usually 5-10 times stiffer than the honeycomb core material, causes a considerable relief of the peak bending and shear stresses in the face sheets (located adjacent to the insert). This stress relieving function is achieved because the relatively stiff potting compound acts as an "attractor" on the transverse shear stresses in the sandwich plate.

Based on the results presented herein, as well as the results of extensive parametric studies presented in Refs. ^{9,10}, a set of guidelines for the design of sandwich plates with through-the-thickness inserts has been formulated.

- If possible, the radial extension of the potting compound
 (b_p b_i, see Figure 2) should be about 0.5b_i. This will
 ensure utilisation of the full shear stress transfer capability of the potting, while ensuring maximum relief of the
 face sheet bending and shear stress concentrations at the
 same time.
- If possible, the ratio of the potting stiffness to the honeycomb stiffness E_p/E_h should be chosen so that $E_p/E_h \approx 3-4$. This will ensure a good compromise between the peak stress level in the face sheets and in the potting and honeycomb materials.
- The external bending moment load case should generally be avoided. This can be achieved by application of the external loads through groups of inserts, thus converting the bending loads to out-of-plane loads on the inserts.
- As severe stress concentrations in the potting and the adhesive bond lines cannot be avoided, the materials chosen for the potting and adhesive bonds should possess long elongation to failure capability.

The listed design guidelines, which have been derived by use of the high-order sandwich plate theory presented herein, generally agree well with the recommendations specified in for instance the ESA *Insert Design Handbook* ¹².

CONCLUSIONS

A high-order sandwich plate theory has been developed and adapted for the analysis of sandwich plates with inserts. The formulation presented herein was developed for sandwich plates with potted through-the-thickness inserts, but it can be extended and adapted for the analysis of sandwich plates with inserts of the fully potted and partially potted types. Mathematically, the insert–sandwich plate problems appear

as sets of first-order partial differential equations, which can be solved numerically in a convenient and cost effective manner using the multi-segment method of integration.

Modules for the analysis of sandwich plates with throughthe-thickness, fully potted and partially potted inserts (under general load conditions), based on the presented high-order sandwich plate theory, are currently being included in the software package ESAComp[®]. ESAComp[®] is a software package for the analysis and design of composite laminates and structural elements, which is under development for the European Space Agency¹³.

ACKNOWLEDGEMENTS

Part of the work presented in this paper was carried out during the period of a research fellowship awarded to O.T. Thomsen with the European Space Agency (ESA), European Space Research and Technology Centre (ESTEC), Structures and Mechanisms Division in Noordwijk, the Netherlands.

APPENDIX

A. DERIVATION OF CORE DISPLACEMENT AND STRESS DISTRIBUTIONS

A1. Basic assumptions

The core material is assumed to be a special type of transversely isotropic solid only possessing stiffness in the through-the-thickness direction, and with the plane of isotropy parallel with the core middle plane (i.e. the in-plane stretching and shearing stiffnesses are assumed to be negligible). Thus, the core material is modelled as a weak or compliant core, as discussed by Librescu⁵. Consequently, the in-plane stress components are nil (see *Figure 3* for coordinates):

$$\sigma_r = \sigma_\theta = \tau_{r\theta} \equiv 0 \tag{A.1}$$

Adopting eqn (A.1), the core equilibrium conditions read

$$\tau_{rz,z} = 0 \tag{A.2}$$

$$\tau_{\theta_{7/7}} = 0 \tag{A.3}$$

$$\sigma_{c,z} + \tau_{rz,r} + \frac{1}{r}\tau_{rz} + \frac{1}{r}\tau_{\theta z,\theta} = 0$$
 (A.4)

From eqns (A.2) and (A.3) it follows that

$$\tau_{rz}(r, \theta, z_c) = \tau_{rz}(r, \theta) \tag{A.5}$$

$$\tau_{\theta z}(r, \theta, z_{c}) = \tau_{\theta z}(r, \theta)$$
 (A.6)

i.e. the shear stresses τ_{rz} and $\tau_{\theta z}$ are predicted to be constant through the thickness of the core.

It is further assumed that the core material behaves in a linear elastic manner, and that only small displacements (negligible rotations) are considered. Given these additional

$$w_c(r, \theta, c/2) = w^1(r, \theta); \quad w_c(r, \theta, -c/2) = w^2(r, \theta)$$

restrictive assumptions, the core constitutive equations and the core kinematic relations can be expressed as (where $\sigma_c = \sigma_z$ in the core):

$$\sigma_{\rm c} = E_{\rm c} \varepsilon_{\rm z} \tag{A.7}$$

$$\tau_{rz} = G_{rz} \gamma_{rz} \tag{A.8}$$

$$\tau_{\theta z} = G_{\theta z} \gamma_{\theta z} \tag{A.9}$$

$$\varepsilon_z = w_{c,z} \tag{A.10}$$

$$\tau_{rz} = w_{c,r} + u_{c,r}$$
 (A.11)

$$\tau_{\theta z} = v_{c,z} + \frac{1}{r} w_{c,\theta}$$
 (A.12)

Combination of eqns (A.7), (A.8), (A.9), (A.10), (A11) and (A.12) yields

$$\sigma_{\rm c} = E_{\rm c} w_{\rm c,z} \tag{A.13}$$

$$\tau_{rz} = G_{rz} \{ w_{c,r} + u_{c,z} \} \tag{A.14}$$

$$\tau_{\theta z} = G_{\theta z} \left\{ v_{c,z} + \frac{1}{r} w_{c,\theta} \right\}$$
 (A.15)

In eqns (A.10), (A.11), (A.12), (A.13), (A.14) and (A.15) w_c represents the transverse displacement of the core material, and u_c and v_c represent the radial and circumferential core displacement components respectively. E_c is the transverse elastic core modulus of the core (z_c direction), and G_{rz} , $G_{\theta z}$ are the transverse core shear moduli (in cylindrical coordinates).

The core material (see *Figure 2*) is assumed to be of honeycomb type, which is most conveniently described as an orthotropic material in Cartesian coordinates (characterised by its "W"- and "L"-direction properties: G_W , G_L), and it is not convenient to describe the material in terms of two shear moduli in cylindrical coordinates (G_{rz} , $G_{\theta z}$). Instead, in the honeycomb region, the core material is suggested as being approximated as a transversely isotropic material as follows:

$$G_{rz} \approx G_{\theta z} = G_{c} = G_{h} = \frac{G_{W} + G_{L}}{2}$$
 (A.16)

In the potting-region of the sandwich core, the adoption of only one G-modulus ($G_{\rm c}=G_{\rm p}$) requires no additional comments, as the potting material is isotropic.

A2. z_c -dependence of displacement and stress fields

By integration of eqn (A.13) with respect to the core thickness coordinate between limits $z_{\rm c} = c/2$ (c is the core thickness, see *Figures 2* and 3) and $z_{\rm c}$ (using integration by parts and using eqn (A.9)), and by requiring continuity of the transverse displacements across the interfaces between the core and the face sheets*, the following is obtained:

$$w_{c,z} = \frac{\sigma_c}{E_c} \Leftrightarrow \int_{c/2}^{z_c} dw_c = \int_{c/2}^{z_c} \frac{\sigma_c}{E_c} dz \Leftrightarrow w_c(r, \theta, z_c)$$

$$= w^1 + \frac{1}{E_c} \left\{ z_c \sigma_c(r, \theta, z_c) - \frac{c}{2} \sigma_c(r, \theta, c/2) \right\}$$

$$+ \frac{1}{E_c} \left\{ \tau_{rz,r} + \frac{1}{r} \tau_{rz} + \frac{1}{r} \tau_{\theta z, \theta} \right\} \left\{ \frac{z_c^2}{2} - \frac{c^2}{8} \right\}$$
(A.17)

^{*}The following conditions are required to be fulfilled:

where $w^1 = w^1(r, \theta)$ is the transverse displacement of the top face (face 1).

Inserting $z_{\rm c} = -c/2$ (corresponding to the bottom surface of the core) in eqn (A.17), and requiring continuity of the transverse displacements of the bottom face sheet and the core, yields

$$w_c(r, \theta, -c/2) = w^1$$

$$+\frac{1}{E_{c}}\left\{-\frac{c}{2}\sigma_{c}(r, \theta, -c/2) - \frac{c}{2}\sigma_{c}(r, \theta, c/2)\right\}$$

$$\Leftrightarrow \sigma_{c}(r, \theta, -c/2) + \sigma_{c}(r, \theta, c/2) = \frac{2E_{c}}{c} \{w^{1} - w^{2}\}$$
 (A.18)

where $w^2 = w^2(r, \theta)$ is the transverse displacement of the bottom face (face 2).

Integration of eqn (A.4) and utilising eqns (A.5) and (A.6) yields

$$\sigma_{c,z} = -\left\{\tau_{rz,r} + \frac{1}{r}\tau_{rz} + \frac{1}{r}\tau_{\theta z,\theta}\right\}$$

$$\Leftrightarrow \int_{c/2}^{z_c} d\sigma_c = -\left\{\tau_{rz,r} + \frac{1}{r}\tau_{rz} + \frac{1}{r}\tau_{\theta,z,\theta}\right\} \int_{c/2}^{z_c} dz$$

$$\Leftrightarrow \sigma_c(r, \theta, z_c) - \sigma_c(r, \theta, c/2)$$

$$= -\left\{\tau_{rz,r} + \frac{1}{r}\tau_{rz} + \frac{1}{r}\tau_{\theta z,\theta}\right\} \left\{z_c - \frac{c}{2}\right\}$$
(A.19)

Setting $z_c = -c/2$ in eqn (A.19):

$$\sigma_{c}(r, \theta, -c/2) - \sigma_{c}(r, \theta, c/2) = \left\{ \tau_{rz, r} + \frac{1}{r} \tau_{rz} + \frac{1}{r} \tau_{\theta z, \theta} \right\} c$$
(A.20)

By addition of eqn (A.20) and eqn (A.18) the following is obtained:

$$\sigma_{c}(r, \theta, -c/2) = \frac{E_{c}}{c} \left\{ w^{1} - w^{2} \right\} + \left\{ \tau_{rz, r} + \frac{1}{r} \tau_{rz} + \frac{1}{r} \tau_{\theta z, \theta} \right\} \frac{c}{2}$$
(A.21)

†By requiring fulfilment of

$$u_c(r, \theta, c/2) = u_r^1(r, \theta, -f_1/2);$$

 $u_c(r, \theta, -c/2) = u_r^2(r, \theta, f_2/2)$

‡ Adopting the classic Kirchhoff assumptions, the face sheet kinematic relations read

$$w_{,r}^{1} = -\beta_{r}^{1}; \quad w_{,r}^{2} = -\beta_{r}^{2}$$

 $u_{r}^{1}(r, \theta, -f_{1}/2) = u_{0r}^{1} - \frac{f_{1}}{2}\beta_{r}^{1}$

§ By requiring fulfilment of

$$v_{c}(r, \theta, c/2) = u_{\theta}^{1}(r, \theta, -f_{1}/2);$$

 $v_{c}(r, \theta, -c/2) = u_{\theta}^{2}(r, \theta, f_{2}/2)$

Adopting the classic Kirchhoff assumptions, the face sheet kinematic relations read

$$\frac{1}{r}w_{,\theta}^{1} = -\beta_{\theta}^{1}; \quad \frac{1}{r}w_{,\theta}^{2} = -\beta_{\theta}^{2}$$
$$u_{\theta}^{1}(r, \theta, -f_{1}/2) = u_{0\theta}^{1} - \frac{f_{1}}{2}\beta_{\theta}^{1}$$

whereas subtraction of eqn (A.20) from eqn (A.18) yields

$$\sigma_{c}(r, \theta, c/2) = \frac{E_{c}}{c} \{w^{1} - w^{2}\} - \left\{\tau_{rz, r} + \frac{1}{r} \tau_{rz} + \frac{1}{r} \tau_{\theta z, \theta}\right\} \frac{c}{2}$$
(A.22)

Inserting eqn (A.22) into eqn (A.19) gives the desired expression for $\sigma_c(r, \theta, z_c)$:

$$\sigma_{c}(r, \theta, z_{c}) = \frac{E_{c}}{c} \left\{ w^{1} - w^{2} \right\} - \left\{ \tau_{rz, r} + \frac{1}{r} \tau_{rz} + \frac{1}{r} \tau_{\theta z, \theta} \right\} z_{c}$$
(A.23)

Inserting eqns (A.22) and (A.23) in the derived expression for $w_c(r, \theta, z_c)$ (given by eqn (A.17)) yields

$$w_{c}(r, \theta, z_{c}) = w^{1} + \frac{\{w^{1} - w^{2}\}}{c} \left\{ z_{c} - \frac{c}{2} \right\}$$
$$-\frac{1}{2E_{c}} \left\{ \tau_{rz, r} + \frac{1}{r} \tau_{rz} + \frac{1}{r} \tau_{\theta_{z}, \theta} \right\} \left\{ z_{c}^{2} - \frac{c^{2}}{4} \right\}$$
(A.24)

from which it is observed that w_c varies as a quadratic function through the core.

The $z_{\rm c}$ dependency of the radial core displacement component $u_{\rm c}$ can be derived by integrating eqn (A.14) with respect to the transverse coordinate (between limits $z_{\rm c}=c/2$ and $z_{\rm c}$). In the computations, eqn (A.24) has been utilised, fulfilment of continuity of the radial displacements across the core–face sheet interfaces† has been required, and the face sheet kinematic relations‡ have been used:

$$u_{c,z} = \frac{\tau_{rz}}{G_c} - w_{c,r} \Leftrightarrow$$

$$u_{c,z} = \frac{\tau_{rz}}{G_c} - w_{,r}^1 - \frac{\{w_{,r}^1 - w_{,r}^2\}}{c} \left\{ z_c - \frac{c}{2} \right\}$$

$$+ \frac{1}{2E_c} \left\{ \tau_{rz,rr} + \frac{1}{r} \tau_{rz,r} - \frac{1}{r^2} \tau_{rz} + \frac{1}{r} \tau_{\theta z,\theta r} - \frac{1}{r^2} \tau_{rz,\theta} \right\}$$

$$\times \left\{ z_c^2 - \frac{c^2}{4} \right\} \Leftrightarrow$$

$$u_c(r, \theta, z_c) = u_{0r}^1 - \frac{\beta_r^1}{2} \left\{ f_1 - \frac{z_c^2}{c} - z_c + \frac{3c}{4} \right\} - \frac{\beta_r^2}{2}$$

$$\times \left\{ \frac{z_c^2}{c} - z_c + \frac{c}{4} \right\} + \frac{\tau_{rz}}{G_c} \left\{ z_c - \frac{c}{2} \right\}$$

$$+ \frac{1}{2E_c} \left\{ \tau_{rz,rr} + \frac{1}{r} \tau_{rz,r} - \frac{1}{r^2} \tau_{rz} + \frac{1}{r} \tau_{\theta z,\theta r} - \frac{1}{r^2} \tau_{\theta z,\theta} \right\}$$

$$\times \left\{ \frac{z_c^3}{c} - \frac{c^2 z_c}{4} + \frac{c^3}{12} \right\}$$
(A.25)

eqn (A.25) shows that u_c varies as a cubic function through the core.

Similar to the derivations shown for u_c , the z_c – dependency of the circumferential core displacement v_c can be found. By integrating eqn (A.15) with respect to z_c , utilising eqn (A.24) again, requiring continuity of the circumferential displacements across the core–face sheet interfaces \S , as well as using the face sheet kinematic

relations, the following is obtained:

$$v_{c,z} = \frac{\tau_{\theta z}}{G_{c}} - \frac{1}{r} w_{c,\theta} \Leftrightarrow$$

$$v_{c,z} = \frac{\tau_{\theta z}}{G_{c}} - \frac{1}{r} w_{,\theta}^{1} - \frac{\{w_{,\theta}^{1} - w_{,\theta}^{2}\}}{rc} \left\{ z_{c} - \frac{c}{2} \right\}$$

$$+ \frac{1}{2rE_{c}} \left\{ \tau_{rz,r\theta} + \frac{1}{r} \tau_{rz,\theta} + \frac{1}{r} \tau_{\theta z,\theta\theta} \right\} \left\{ z_{c}^{2} - \frac{c^{2}}{4} \right\} \Leftrightarrow$$

$$v_{c}(r, \theta, z_{c}) = u_{0\theta}^{1} - \frac{\beta_{,\theta}^{1}}{2} \left\{ f_{1} - \frac{z_{c}^{2}}{c} - z_{c} + \frac{3c}{4} \right\}$$

$$- \frac{\beta_{,\theta}^{2}}{2} \left\{ \frac{z_{c}^{2}}{c} - z_{c} + \frac{c}{4} \right\} + \frac{\tau_{\theta z}}{G_{c}} \left\{ z_{c} - \frac{c}{2} \right\}$$

$$+ \frac{1}{2rE_{c}} \left\{ \tau_{rz,r\theta} + \frac{1}{r} \tau_{rz,\theta} + \frac{1}{r} \tau_{\theta z,\theta\theta} \right\}$$

$$\times \left\{ \frac{z_{c}^{3}}{c} - \frac{c^{2}z_{c}}{4} + \frac{c^{3}}{12} \right\}$$
(A.26)

As was the case for u_c , it is observed that v_c varies as a cubic function through the core.

B. COMPLETE SET OF GOVERNING EQUATIONS

B1. Governing equations for the top face sheet

$$u_{0r,r}^{1} = -\frac{\nu_{1}}{r}u_{0r}^{1} - \frac{\nu_{1}}{r}u_{0\theta,\theta}^{1} + \frac{N_{r}^{1}}{A_{1}}$$
 (B.1)

$$u_{0\theta,r}^{1} = -\frac{1}{r}u_{0r,\theta}^{1} + \frac{1}{r}u_{0\theta}^{1} + \frac{N_{r\theta}^{1}}{A_{1}(1-\nu_{1})}$$
(B.2)

$$w_r^1 = -\beta_r^1 \tag{B.3}$$

$$\beta_{r,r}^{1} = -\frac{\nu_{1}}{r}\beta_{r}^{1} - \frac{\nu_{1}}{r}\beta_{\theta,\theta}^{1} + \frac{M_{r}^{1}}{D_{r}}$$
 (B.4)

$$\beta_{\theta,r}^{1} = \frac{M_{r\theta}^{1}}{D_{1}(1-\nu_{1})} \tag{B.5}$$

$$N_{r,r}^{1} = \frac{A_{1}(1-\nu_{1}^{2})}{r^{2}}u_{0r}^{1} + \frac{A_{1}(1-\nu_{1}^{2})}{r^{2}}u_{0\theta,\theta}^{1} - \frac{(1-\nu_{1})}{r}N_{r}^{1}$$
$$-\frac{1}{r}N_{r\theta,\theta}^{1} + \tau_{zr}$$
(B.6)

$$N_{r\theta,r}^{1} = -\frac{A_{1}(1-\nu_{1}^{2})}{r^{2}}u_{0r,\theta}^{1} - \frac{A_{1}(1-\nu_{1}^{2})}{r^{2}}u_{0\theta,\theta\theta}^{1} - \frac{\nu_{1}}{r}N_{r,\theta}^{1}$$
$$-\frac{2}{r}N_{r\theta}^{1} + \tau_{z\theta}$$
(B.7)

$$M_{r,r}^{1} = \frac{D_{1}(1-\nu_{1}^{2})}{r^{2}} \beta_{r}^{1} + \frac{D_{1}(1-\nu_{1}^{2})}{r^{2}} \beta_{\theta,\theta}^{1} - \frac{(1-\nu_{1})}{r} M_{r}^{1}$$
$$-\frac{1}{r} M_{r\theta,\theta}^{1} + Q_{r}^{1} - \frac{f_{1}}{2} \tau_{zr}$$
(B.8)

$$M_{r\theta,r}^{1} = -\frac{D_{1}(1-\nu_{1})\nu_{1}}{r^{2}}\beta_{r,\theta}^{1} - \frac{D_{1}(1-\nu_{1})\nu_{1}}{r^{2}}\beta_{\theta,\theta\theta}^{1} + \frac{(1-\nu_{1})}{r}M_{r,\theta}^{1} - \frac{2}{r}M_{r\theta}^{1} - \frac{f_{1}}{2}\tau_{z\theta}$$
(B.9)

$$\begin{split} Q_{r,r}^{1} &= \frac{E_{c}}{c} \, w^{1} - \frac{D_{1}(1-\nu_{1})}{r^{3}} \, \beta_{r,\,\theta\theta}^{1} - \frac{D_{1}(1-\nu_{1})}{r^{3}} \, \beta_{\theta,\,\theta\theta\theta}^{1} \\ &- \frac{1}{r^{2}} M_{r,\,\theta\theta}^{1} - \frac{1}{r} \, Q_{r}^{1} - \frac{c}{2r} \, \tau_{rz} - \frac{c}{2} \, q_{r} - \frac{c}{2r} \, \tau_{\theta z,\,\theta} - \frac{E_{c}}{c} \, w^{2} \end{split} \tag{B.10}$$

B2. Governing equations for the core

$$\tau_{rz,r} = q_r$$

$$q_{r,r} = -\frac{12E_c}{c^3} u_{0r}^1 + \frac{6E_c(f_1 + c)}{c^3} \beta_r^1 + \left\{ \frac{1}{r^2} + \frac{12E_c}{c^2 G_c} \right\} \tau_{rz}$$

$$-\frac{1}{r} q_r + \frac{1}{r^2} \tau_{\theta z, \theta} - \frac{1}{r} q_{\theta, \theta} + \frac{12E_c}{c^3} u_{0r}^2 + \frac{6E_c(f_2 + c)}{c^3} \beta_r^2$$
(B.12)

$$\tau_{\theta z, r} = q_{\theta} \tag{B.13}$$

$$q_{\theta,r} = -\frac{G_{c}(3-\nu_{1})}{cr^{2}}u_{0r,\theta}^{1} + \frac{2G_{c}}{cr^{2}}u_{0\theta}^{1} - \frac{G_{c}(1-\nu_{1})}{cr^{2}}u_{0\theta,\theta\theta}^{1}$$

$$-\frac{G_{c}(2-\nu_{1})}{crA_{1}(1-\nu_{1})}N_{r,\theta}^{1} + \frac{G_{c}}{crA_{1}(1-\nu_{1})}N_{r\theta}^{1} + \frac{1}{r}q_{r,\theta}$$

$$+\frac{G_{c}}{c}\left\{\frac{1}{A_{1}(1-\nu_{1})} + \frac{1}{A_{2}(1-\nu_{2})}\right\}\tau_{\theta z} - \frac{1}{r}q_{\theta}$$

$$+\frac{G_{c}(3-\nu_{2})}{cr^{2}}u_{0r,\theta} - \frac{2G_{c}}{cr^{2}}u_{0\theta}^{2} + \frac{G_{c}(1-\nu_{2})}{cr^{2}}u_{0\theta,\theta\theta}^{2}$$

$$+\frac{G_{c}(2-\nu_{2})}{crA_{2}(1-\nu_{2})}N_{r,\theta}^{2} - \frac{G_{c}}{crA_{2}(1-\nu_{2})}N_{r\theta}^{2} \qquad (B.14)$$

B3. Governing equations for the bottom face sheet

$$u_{0r,r}^2 = -\frac{\nu_2}{r} u_{0r}^2 - \frac{\nu_2}{r} u_{0\theta,\theta}^2 + \frac{N_r^2}{A_2}$$
 (B.15)

$$u_{0\theta,r}^2 = -\frac{1}{r}u_{0r,\theta}^2 + \frac{1}{r}u_{0\theta}^2 + \frac{N_{r\theta}^2}{A_2(1-\nu_2)}$$
 (B.16)

$$w_r^2 = -\beta_r^2 \tag{B.17}$$

$$\beta_{r,r}^2 = -\frac{\nu_2}{r}\beta_r^2 - \frac{\nu_2}{r}\beta_{\theta,\theta}^2 + \frac{M_r^2}{D_2}$$
 (B.18)

$$\beta_{\theta, r}^2 = \frac{M_{r\theta}^2}{D_2(1 - \nu_2)} \tag{B.19}$$

$$N_{r,r}^{2} = -\tau_{zr} + \frac{A_{2}(1-\nu_{2}^{2})}{r^{2}} u_{0r}^{2} + \frac{A_{2}(1-\nu_{2}^{2})}{r^{2}} u_{0\theta,\theta}^{2}$$
$$-\frac{(1-\nu_{2})}{r} N_{r}^{2} - \frac{1}{r} N_{r\theta,\theta}^{2}$$
(B.20)

$$N_{r\theta,r}^{2} = -\tau_{z\theta} - \frac{A_{2}(1-\nu_{2}^{2})}{r^{2}} u_{0r,\theta}^{2} - \frac{A_{2}(1-\nu_{2}^{2})}{r^{2}} u_{0\theta,\theta\theta}^{2}$$
$$-\frac{\nu_{2}}{r} N_{r,\theta}^{2} - \frac{2}{r} N_{r\theta}^{2}$$
(B.21)

$$M_{r,r}^{2} = -\frac{f_{2}}{2} \tau_{zr} + \frac{D_{2}(1-\nu_{2}^{2})}{r^{2}} \beta_{r}^{2} + \frac{D_{2}(1-\nu_{2}^{2})}{r^{2}} \beta_{\theta,\theta}^{2}$$
$$-\frac{(1-\nu_{2})}{r} M_{r}^{2} - \frac{1}{r} M_{r\theta,\theta}^{2} + Q_{r}^{2}$$
(B.22)

$$M_{r\theta,r}^{2} = -\frac{f_{2}}{2} \tau_{z\theta} - \frac{D_{2}(1-\nu_{2})\nu_{2}}{r^{2}} \beta_{r,\theta}^{2} - \frac{D_{2}(1-\nu_{2})\nu_{2}}{r^{2}} \beta_{\theta,\theta\theta}^{2} + \frac{(1-\nu_{2})}{r} M_{r,\theta}^{2} - \frac{2}{r} M_{r\theta}^{2}$$
(B.23)

$$Q_{r,r}^{2} = -\frac{E_{c}}{c} w^{1} - \frac{c}{2r} \tau_{rz} - \frac{c}{2} q_{r} - \frac{c}{2r} \tau_{\theta z,\theta} + \frac{E_{c}}{c} w^{2}$$

$$-\frac{D_{2}(1-\nu_{2})}{r^{3}} \beta_{r,\theta\theta}^{2} - \frac{D_{2}(1-\nu_{2})}{r^{3}} \beta_{\theta,\theta\theta\theta}^{2} - \frac{1}{r^{2}} M_{r,\theta\theta}^{2}$$

$$-\frac{1}{r} Q_{r}^{2}$$
(B.24)

In eqns (B.1)–(B.24), ν_i (i = 1, 2) is the Poisson's ratio of the face sheets, and A_i and D_i (i = 1, 2) are the extensional and bending stiffnesses of the face sheets.

REFERENCES

1. Plantema, F.J. Sandwich Construction. Wiley, New York, 1966.

- Allen, H.G. Analysis and Design of Structural Sandwich Panels. Pergamon Press, Oxford, 1969.
- Stamm, K. and Witte, H. Sandwichkonstruktionene. Springer, Wien, Austria, 1974 (in German).
- Zenkert, D. An Introduction to Sandwich Construction. Chameleon Press, London, 1995.
- Librescu, L., Elastostatics and Kinetics of Anistropic and Heterogeneous Shell-Type Structures. Noordhoff, Leyden, 1975.
- Frostig, Y. and Baruch, M., Bending of sandwich beams with transversely flexible core. AIAA Journal, 1990, 28, 523–531.
- Frostig, Y., On stress concentration in the bending of sandwich beams with transversely flexible core. *Composite Structures*, 1993, 24, 161–169.
- Frostig, Y. and Shenhar, Y., High-order bending of sandwich beams with a transversely flexible core and unsymmetrical laminated composite skins. *Composites Engineering*, 1995, 5, 405–414.
- Thomsen, O.T. Analysis of sandwich plates with through-the-thickness inserts using a high-order sandwich plate theory. ESA/ESTEC Report EWP-1807, Noordwijk, The Netherlands, 1994.
- Thomsen, O.T., Analysis of sandwich plates with fully potted inserts using a high-order sandwich plate theory. ESA/ESTEC Report EWP-1827, Nordwijk, The Netherlands, 1995.
- Kalnins, A., Analysis of shells of revolution subjected to symmetrical and nonsymmetrical loads. *Transactions of the* ASME Journal of Applied Mechanics, 1964, 31, 467–476.
- European Space Agency. Insert Design Handbook, ESA PSS-03-1202, Issue 1, 1987.
- Saarela, O., Palantera, M., Haberle, J. and Klein, M., ESACOMP: a
 powerful tool for the analysis and design of composite materials.

 Proceedings of the International Symposium on Advanced
 Materials for Lightweight Structures (ESA-WPP-070), ESTEC,
 Noordwijk, March 1994, pp. 161–169.